Inorg. Chem. **2008**, *47*, 7868−7873

Chemical Stability of ZnO Nanostructures in Simulated Physiological Environments and Its Application in Determining Polar Directions

Chun Cheng,[†] Renlong Xin,[‡] Yang Leng,[‡] Dapeng Yu,[§] and Ning Wang*[,†]

Department of Physics and the Institute of Nano Science and Technology, The Hong Kong University of Science and Technology, Hong Kong, P.R. China, Department of Mechanical Engineering, The Hong Kong University of Science and Technology, Hong Kong, P.R.China, and Department of Physics, Peking University, Beijing, P.R. China

Received March 23, 2008

The in vitro chemical stability and etching of ZnO nanostructures in simulated physiological solution (SPS) were studied using electron microscopy. Calcium hydrogen phosphate thin layers were observed to be uniformly deposited on the surfaces of ZnO nanomaterials in SPS. Electron diffraction and high-resolution transmission electron microscopy revealed that the calcium hydrogen phosphate layers were amorphous and had excellent interfacial contact with the nanocrystals. ZnO nanostructures fabricated by thermal evaporation were found to survive much longer in SPS than those fabricated using a hydrothermal solution method. The shapes of the voids formed in the ZnO nanostructures by the etching in SPS can be used to deduce the polar directions of ZnO nanostructures.

Introduction

Biosensors based on nanostructured materials such as nanowires[1–5] and nanotubes[6–9 10] have received increasing attention in recent years. Nanostructures possess high biosensitivity because of the depletion or accumulation of charge carriers on their surfaces when charged biological macromolecules are bound. This surface charge affects the entire cross-sectional conduction pathway.[4] ZnO nanostructures are one type with many potential applications in optoelectronic devices, transducers, and photovoltaic devices.[11–14] Recently, ZnO nanomaterials are being widely investigated for use in biosensors,[15–17] bioimaging,[18,19] drug delivery, [20] and other such biological applications. Such applications often involve direct interaction with biological systems and sometimes require a certain time to perform their functions, for example, in the real time bioimaging of protein interactions or in the real time monitoring of changes in pH or glucose in vivo. This makes investigating the bioactivity, biocompatibility, chemical stability, and behavior of nanomaterials in biofluids a priority. So far, little has been published on the bioactivity and biocompatibility of ZnO nanomaterials[21–24] and, their chemical stability and interactions with biofluids remain poorly understood.

* To whom correspondence should be addressed. E-mail: phwang@ust.hk. Fax: (+) 852-2351652.
[†] Department of Physics and the Institute of Nano Science and Technology, The Hong Kong University of Science and Technology.
[‡] Department of Mechanical Engineering, The Hong Kong University of Science and Technology.
[§] Peking University.

(1) Cui, Y.; Wei, Q.; Park, H.; Lieber, C. M. *Science* **2001**, *293*, 1289.
(2) Wang, W. U.; Chen, C.; Lin, K. H.; Fang, Y.; Lieber, C. M. *Proc. Natl. Acad. Sci. U.S.A.* **2005**, *102*, 3208.
(3) Zheng, G. F.; Patolsky, F.; Cui, Y.; Wang, W. U.; Lieber, C. M. *Nat. Biotechnol.* **2005**, *23*, 1294.
(4) Hahm, J.; Lieber, C. M. *Nano Lett.* **2004**, *4*, 51.
(5) He, H. X.; Tao, N. J. *Adv. Mater.* **2002**, *14*, 161.
(6) Gabriel, J. P.; Bradley, K.; Gruner, G. *Nano Lett.* **2003**, *3*, 459.
(7) Bianco, A.; Prato, M. *Adv. Mater.* **2003**, *15*, 1765.
(8) Wohlstadter, J. N.; Wilbur, J. L.; Sigal, G. B.; Biebuyck, H. A.; Billadeau, M. A.; Dong, L. W.; Fischer, A. B.; Gudibande, S. R.; Jameison, S. H.; Kenten, J. H.; Leginus, J.; Leland, J. K.; Massey, R. J.; Wohlstadter, S. J. *Adv. Mater.* **2003**, *15*, 1184.
(9) Fan, R.; Karnik, R.; Yue, M.; Li, D. Y.; Majumdar, A.; Yang, P. D. *Nano Lett.* **2005**, *5*, 1633.
(10) He, L.; Musick, M. D.; Nicewarner, S. R.; Salinas, F. G.; Benkovic, S. J.; Natan, M. J.; Keating, C. G. *J. Am. Chem. Soc.* **2000**, *122*, 9071.
(11) Wang, Z. L. *J. Phys.: Condens. Matter* **2004**, *16*, 829.
(12) Pan, Z. W.; Dai, Z. R.; Wang, Z. L. *Science* **2001**, *291*, 1947.
(13) Huang, M. H.; Mao, S.; Feick, H.; Yan, H. Q.; Wu, Y. Y.; Kind, H.; Weber, E.; Russo, R.; Yang, P. D. *Science* **2001**, *292*, 1897.
(14) Qin, Y.; Wang, X. D.; Wang, Z. L. *Nature* **2008**, *451*, 809.
(15) Kim, J. S.; Park, W. I.; Lee, C. H.; Yi, G. C. *J. Korean Phys. Soc.* **2006**, *49*, 1635.
(16) Al-Hilli, S. M.; Willander, M.; Ost, A.; Stralfors, P. *J. Appl. Phys.* **2007**, *102*, 084304.
(17) Wei, A.; Sun, X. W.; Wang, J. X.; Lei, Y.; Cai, X. P.; Li, C. M.; Dong, Z. L.; Huang, W. *Appl. Phys. Lett.* **2006**, *89*, 123902.
(18) Dorfman, A.; Kumar, N.; Hahm, J. *Adv. Mater.* **2006**, *18*, 2685.
(19) Wu, Y. L.; Lim, C. S.; Fu, S.; Tok, A. I. Y.; Lau, H. M.; Boey, F. Y. C.; Zeng, X. T. *Nanotechnology* **2007**, *18*, 215604.
(20) Khopade, A. J.; Arulsudar, N.; Khopade, S. A.; Hartmann, J. *Biomacromolecules* **2005**, *6*, 229.

10.1021/ic8005234 CCC: $40.75
Published on Web 07/30/2008

Table 1. Ion Concentrations of SPS

ion	Na^+	K^+	Mg^{2+}	Ca^{2+}	Cl^-	HCO_3^-	HPO_4^{2-}	SO_4^{2-}
concentrations (mmol\dm^3)	142.0	5.0	1.5	2.5	103.0	27.0	1.0	0.5

Wurtzite ZnO has been shown to form structures such as nanowires, nanobelts,[12] nanorings,[25] nanosprings,[26] and nanohelices.[27] It is believed that the polar surfaces (Zn terminated or O terminated) play an important role in the formation of these nanostructures. The differently charged surfaces show distinct reactivity and thus display different growth behaviors. To correlate the growth behaviors with the structure of nanosized crystalline ZnO, it is important to identify the polarity of the ZnO nanocrystals experimentally. This has been the first study of the in vitro chemical stability of ZnO nanostructures with different morphologies and their etching behavior in simulated physiological solution (SPS) with ion concentrations approximately equal to those in human blood plasma. SPS has been used widely for in vitro assessment of the artificial biomaterials.[28] ZnO nanomaterials synthesized by thermal evaporation and solution methods have different "survival times" in SPS, and they show interesting anisotropic etching behaviors. The anisotropic etching behaviors can be very useful for determining the polar directions of ZnO nanostructures.

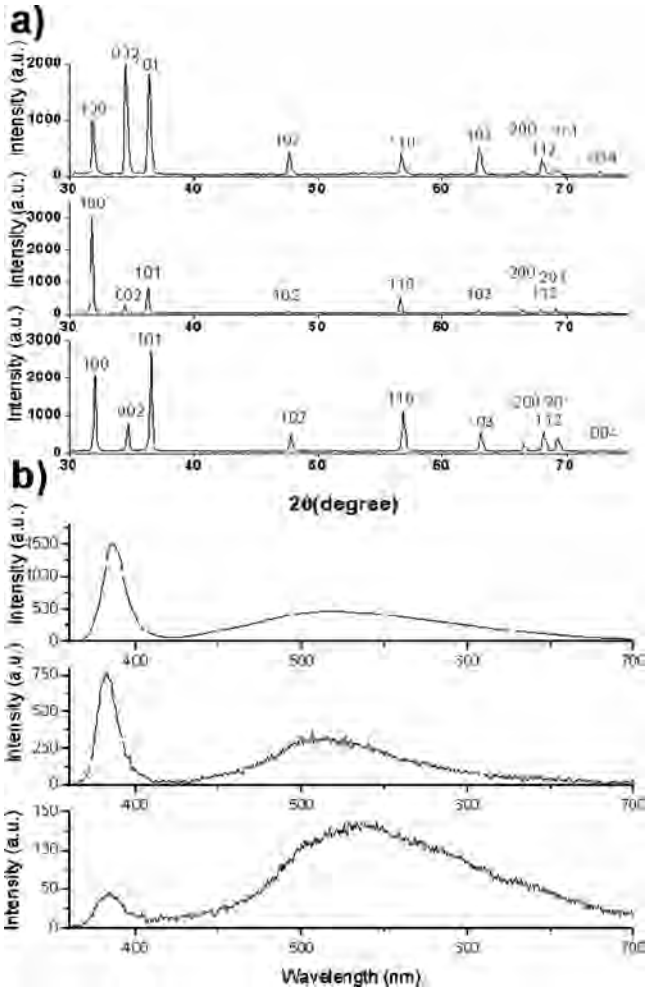

Figure 1. (a) XRD patterns of ZnO nanowires fabricated by the hydrothermal method (bottom) and nanowires (middle) /nanobelts (top) by thermal vapor deposition. (b) PL spectra of ZnO nanowires fabricated by the hydrothermal method (bottom) and nanowires (middle) /nanobelts (top) by the thermal vapor deposition.

Experimental Section

Preparation of ZnO Nanostructures. ZnO nanowires and nanoribbons with different morphologies were fabricated by (1) a simple thermal evaporation method based on the self-catalyzed vapor-solid mechanism (no metal catalyst was used); and (2) a simple hydrothermal method without using any capping agents or surfactants. In brief, ZnO powder was placed at the center of an evacuated (2×10^{-2} torr) tube furnace. Substrates were placed downstream in a lower temperature region (400−800 °C) of the furnace. The furnace was heated to 1400 °C for 2 h. For the growth of ZnO nanowires and nanobelts, carbon foils and a polycrystalline sapphire substrate were used, respectively. In the solution hydrothermal method, 5 mL of 0.1 M zinc acetate ethanol solution was mixed with 35 mL of 0.5 M NaOH ethanol solution to form a mixed

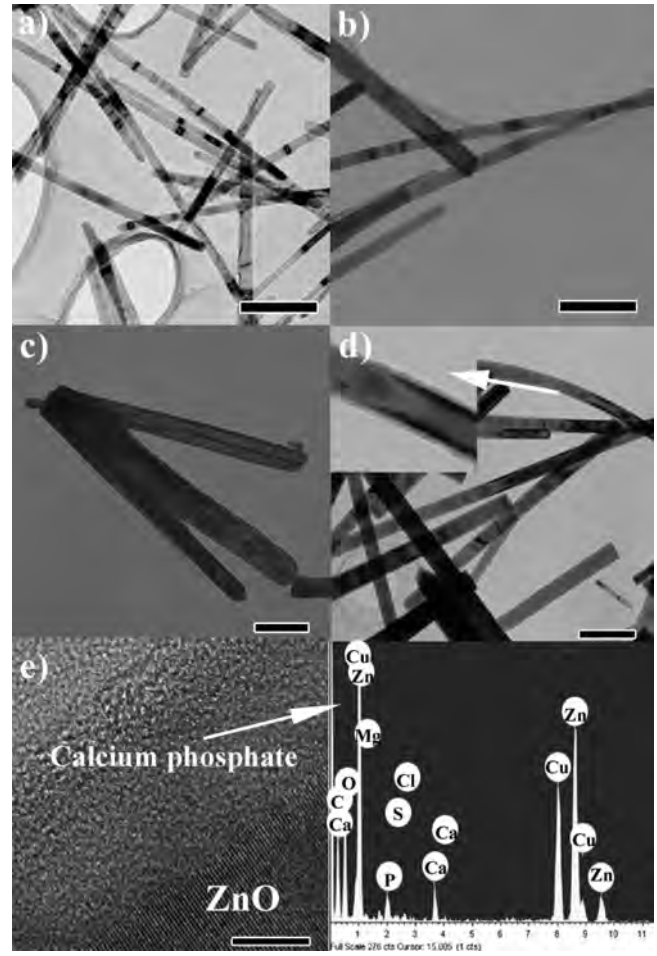

Figure 2. (a) ZnO nanowires fabricated by the hydrothermal method. (b) ZnO nanowires fabricated by thermal evaporation. (c) Amorphous thin calcium phosphate shells formed on the surfaces of the ZnO nanowires synthesized by the hydrothermal method. These ZnO nanowires acted as the templates. (d) Calcium phosphate shells coated on the ZnO nanowires synthesized by thermal evaporation. (e) HRTEM image of calcium phosphate shell-ZnO nanowire structures and the EDS spectrum of the calcium phosphate shell. Scale bars 200 nm for panels a and b, 100 nm for panels c and d, and 5 nm for panel e.

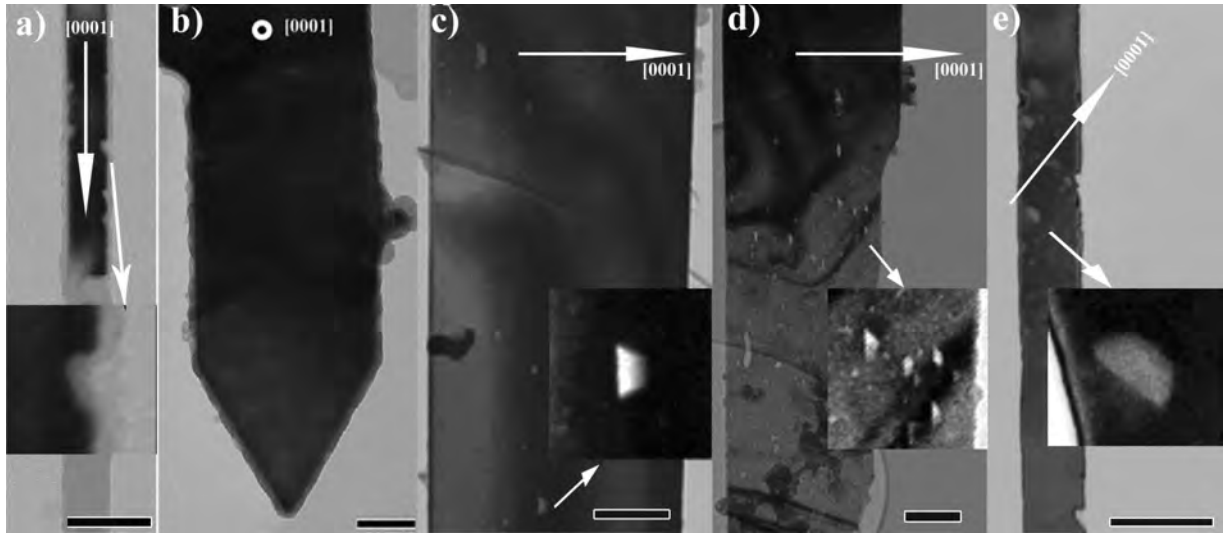

Figure 3. TEM images of etched ZnO nanostructures: (a) nanowires viewed along $[1\bar{1}00]$; (b) nanobelts with a (0001) dominant plane; (c) and (e) with a $(1\bar{1}00)$ dominant plane; (d) with a $(11\bar{2}0)$ dominant plane. Scale bar 50 nm for panels a and b; 200 nm for panels c−e.

solution which was later transferred into a Teflon-lined stainless steel autoclave (50 mL) and heated to 180 °C. After 24 h, a white precipitate had formed at the bottom of the autoclave with transparent solution above the product.

Characterization. The as-prepared samples were characterized by X-ray diffraction (XRD; Philips, PW1813). A drop of solution containing the nanostructures was diluted with ethanol and sonicated for 15 min. The nanostructures were then dispersed onto a holey carbon film for structural characterization using a JEOL JEM-2010F transmission electron microscope (TEM) equipped with an energy-dispersive X-ray spectrometer (EDS). The convergent-beam electron diffraction (CBED) patterns were recorded using a Philips TEM (CM120), and the CBED simulation was performed using the JEMS software. The photoluminescence (PL) measurements were carried out using a He−Cd laser as the exciting light source.

In Vitro Experiments. The in vitro experiments were conducted in the SPS[28] which has the same ionic composition as human plasma. One liter of SPS was prepared by dissolving 5.403 g of NaCl, 0.736 g of $NaHCO_3$, 2.036 g of Na_2CO_3, 0.225 g of KCl, 0.182 g of K_2HPO_4, 0.310 g of $MgCl_2 \cdot 6H_2O$, 11.928 g of HEPES (2-(4-(2-hydroxyethyl)-1-piperazinyl) ethane surfonic acid), 0.293 g of $CaCl_2$, 0.072 g of Na_2SO_4, and 1.5 mL of 1 mol·L^{-1} NaOH into double distilled water in sequence. The ion concentrations of this SPS are listed in Table 1. ZnO nanomaterials were immersed in SPS at 37 °C for several hours to several weeks. After this treatment, the ZnO nanomaterial samples were washed with distilled water and dispersed on holey carbon supporting grids for structural characterization by transmission electron microscopy.

Results and Discussions

As shown in the XRD data in Figure 1a, ZnO nanowires and nanobelts synthesized by our methods can be well indexed as Wurtzite ZnO. The lattice parameters calculated for the nanowires from the hydrothermal method are $a = 0.324$ nm and $c = 0.518$ nm, and the nanowires and nanobelts from thermal evaporation show very similar lattice parameters ($a = 0.324$ nm and $c = 0.520$ nm). The diffraction peaks are sharp and no other phases can be found. This indicates that these nanostructures have very good crystallinity. It has been widely acknowledged that point defects, for example, oxygen vacancies and impurity atoms, are the main defects in ZnO nanocrystals that cannot be detected by electron microscopy. However, these point defects largely affect the optical properties such as PL.[29] So far, there is no good way to determine the defect types and numbers quantitatively in nanostructured materials. However, the presence of impurities or point defects in ZnO nanostructures can be revealed by a PL spectrum.[29] Figure 1b shows the PL results obtained from the as-prepared ZnO nanostructures. The nanostructures from the hydrothermal method have a large green emission (due to defects, ranging from 450 to 650 nm) versus the band gap emission (near 380 nm) compared to those nanostructures from the thermal evaporation method, indicating that the point defect concentration (such as ionized oxygen vacancies, antisite oxygen and zinc interstitials, etc.)[29] is high in the hydrothermal samples. In addition, according to the band gap emission intensity, the ZnO nanostructures from the thermal evaporation method have a high crystalline quality.

Figures 2a,b are TEM images showing the morphologies of as-grown ZnO nanowires synthesized by the hydrothermal solution method and the thermal evaporation process, respectively. The nanowires from these two synthesis methods show uniform diameters of about 30 nm and smooth surfaces with a unique [0001] growth direction. According to the electron diffraction patterns and high-resolution TEM (HRTEM) images taken from these nanowires, the nanowires contained few defects and showed high crystallinity. Figures 2c,d are low-magnification TEM images of nanowires after they had been soaked in SPS for 3 days. Most ZnO nanowires synthesized by the hydrothermal solution method were etched out, leaving only thin tubular shells several nanometers thick, as shown in Figure 2c. These shells apparently formed on the wire surface. However, the nanowires fabricated by thermal evaporation were stable and still held their original shapes after soaking, with some voids several nanometers in diameter randomly distributed on their surface (see Figure 2d). The wires formed through the high temperature process may have been able to persist longer in the SPS solution

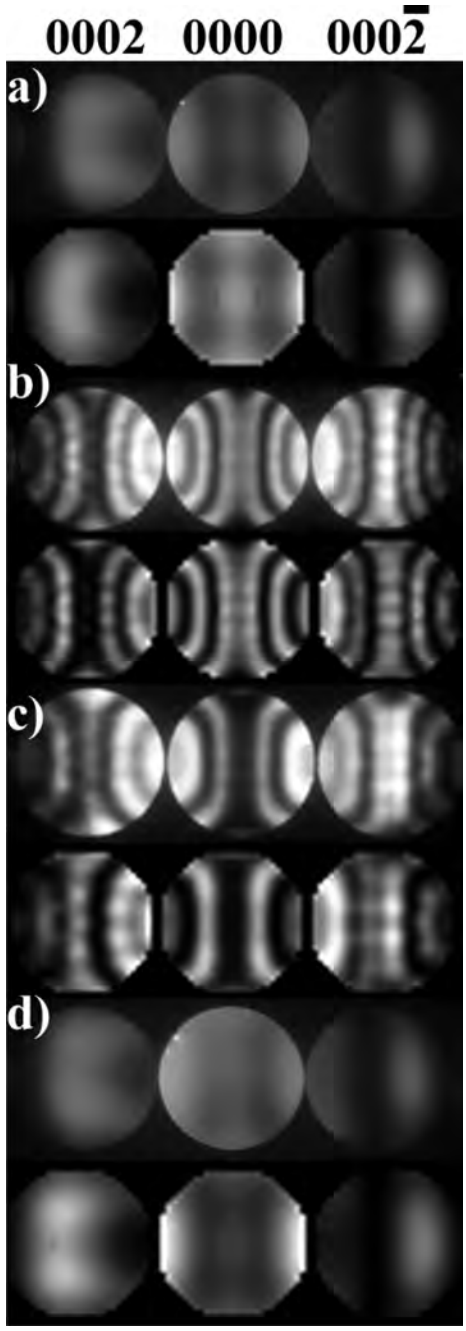

Figure 4. CBED experimental patterns (top) and simulated patterns (bottom) for the samples shown in Figures (a) 3a,b; (b) Figure 3c; (c) Figure 3d; and (d) Figure 3e.

because they had better crystalline quality than the nanowires formed through the hydrothermal process as revealed by our PL studies (Figure 1b). ZnO nanowires fabricated by thermal evaporation were observed to survive in SPS at least two weeks.

As is illustrated in the inset of Figure 2d, a very thin layer (several nanometers in thickness) uniformly coated each ZnO nanowire after immersion. Selected-area electron diffraction and HRTEM (Figure 2e) demonstrated that these thin shells were amorphous. The results from EDS study indicated that the shells contained a high concentration of phosphorus (3.27%, at) (atomic percent) and calcium (2.86%, at). Other impurities such as Mg (0.17%, at), S (0.52%, at), and Cl (0.99%, at) in SPS were also detected. Some very weak peaks are caused by the background noise and cannot be characterized by peaks from any elements. The amorphous calcium phosphate is a precursor of hydroxyapatite and can be stabilized by being crystallized into apatite.[30,31] Biomedical researchers commonly use the formation of apatite on materials soaked in SPS to indicate the material's bioactivity. The precipitation of amorphous calcium phosphate in these experiments shows that ZnO nanostructures behave as bioactive materials.[31]

When ZnO nanostructures are soaked in SPS, $ZnO(OH)_4^{2-}$ is formed by the reaction $ZnO + 3H_2O = ZnO(OH)_4^{2-} + 2H^+$, resulting in a negatively charged surface. Takadama et al. [30] have explained that such negative surfaces can induce the formation of amorphous calcium phosphate. Calcium ions in the SPS are attracted to the surface preferentially. This is followed by the arrival of HPO_4^{2-}, resulting in a hydrated precursor cluster of calcium hydrogen phosphate. The precursor clusters grow by incorporating calcium and phosphate ions from the surrounding SPS. The calcium phosphate phase accumulates uniformly on the surface, forming a thin shell of amorphous calcium phosphate intimately interfaced with the substrate.[31] The fast reaction for the formation of $ZnO(OH)_4^{2-}$ at defect sites was probably responsible for the obvious etching which formed the voids on the surfaces of the ZnO nanostructures tested in these experiments.

The etching and morphology changes were further studied using HRTEM. All the samples in this phase of the study were fabricated by the thermal evaporation method. Apart from the thin shells of amorphous calcium phosphate, numerous voids were clearly visible by TEM. As Figure 3a shows, the voids at the nanowire surface were shaped approximately as right-angled triangles. (See also the enlarged image in the inset.) Because the voids were rather small, it was hard to distinguish their profile shapes embedded in the nanostructures when the sample was thick. The voids in the nanobelts with {0001} as the dominant plane could be seen only as small "spots" with quite poor contrast at low magnification (Figure 3b). However, the etching patterns could be observed clearly in the nanobelts grown with other dominant planes, such as $(1\bar{1}00)$ and $(11\bar{2}0)$, as shown in Figures 3c−e. In these cases, many voids about several nanometers in size were observed all over the

(21) Sayes, C. M.; Reed, K. L.; Warheit, D. B. *Toxicol. Sci.* **2007**, *97*, 163.
(22) Wesselkamper, S. C.; Chen, L. C.; Gordon, T. *Respir. Res.* **2005**, *6*, 73.
(23) Wang, B.; Feng, W.; Wang, M.; Wang, T.; Gu, Y.; Zhu, M.; Ouyang, H.; Shi, J.; Zhang, F.; Zhao, Y.; Chai, Z.; Wang, H.; Wang, J. *J. Nanopart. Res.* **2008**, *10*, 263.
(24) Zhou, J.; Xu, N. S.; Wang, Z. L. *Adv. Mater.* **2006**, *18*, 2435.
(25) Kong, X. Y.; Ding, Y.; Yang, R.; Wang, Z. L. *Science* **2004**, *303*, 1348.
(26) Kong, X. Y.; Wang, Z. L. *Nano Lett.* **2003**, *3*, 1625.
(27) Gao, P. X.; Ding, Y.; Mai, W. J.; Hughes, W. L.; Lao, C. S.; Wang, Z. L. *Science* **2005**, *309*, 1700.
(28) Kim, H. M.; Miyazaki, T.; Kokubo, T.; Nakamura, T. *Key Eng. Mater.* **2001**, *47*, 192.
(29) Djurisic, A. B.; Leung, Y. H. *Small* **2006**, *2*, 944.
(30) Takadama, H.; Kim, H. M.; Kokubo, T.; Nakamura, T. *Chem. Mater.* **2001**, *13*, 1108.
(31) Liu, X.; Fu, R. K. Y.; Chu, P. K.; Ding, C. *Appl. Phys. Lett.* **2004**, *85*, 3623.

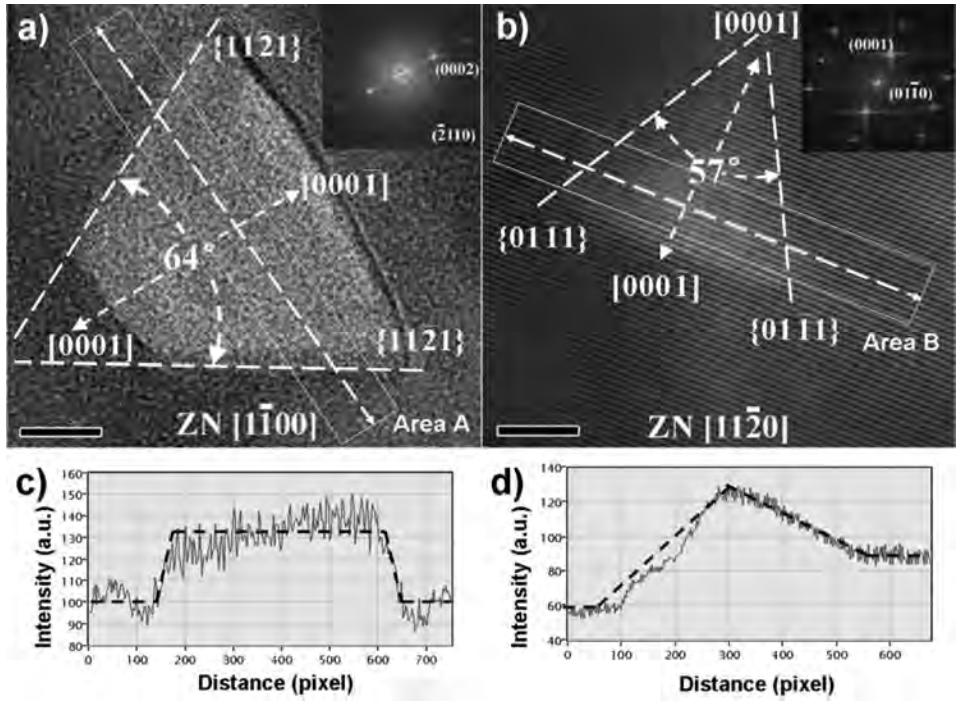

Figure 5. HRTEM images showing the typical morphologies of the voids viewed along (a) [1$\bar{1}$00] and (b) [11$\bar{2}$0] directions. Insets are corresponding Fourier transform patterns. (c, d) Profile graphs of the outlined areas A and B shown in panels a and b. Scale bar 5 nm for panels a and b.

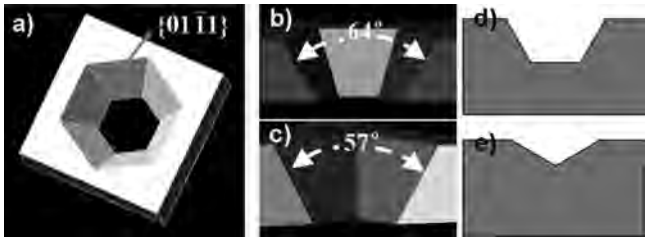

Figure 6. (a) Schematic model of an etched void. (b, c) 3D projections of the voids viewed along the [1$\bar{1}$00] and [11$\bar{2}$0] directions. (d, e) Profile images of cross-sections of panels b and c cut perpendicular to the [0001] direction.

nanobelts. Apart from some irregularly shaped voids, most of the voids in the nanobelts with (1$\bar{1}$00) dominant planes were isosceles trapezoids (see the inset in Figures 3c,e). In nanobelts with (11$\bar{2}$0) dominant planes the voids were triangles (Figure 3d). It is worth noting that the symmetry axes of the void patterns were always along the [0001] direction.

The atomic structure of Wurtzite ZnO has positively and negatively charged polar surfaces due to alternative stacking of O^{2-} and Zn^{2+} ions along the *c* axis. Traditionally, CBED has been widely used to determine the polarity of this kind of compound. However, the sample thickness determines the contrast of CBED diffraction patterns.[25–27,32] CBED patterns taken from nanometer size (<10nm) samples show no useful contrast. To quantitatively determine the polarity of the surfaces, CBED was supplemented by theoretical simulation. Figure 4 shows CBED patterns taken from ZnO nanostructures with the electron beam parallel to the [1$\bar{1}$00] direction. These patterns (shown at the top of Figures 4a−d) match fairly well with the simulated ones (shown at the bottom of Figures 4a−d) produced using the JEMS simulation software. The thicknesses for the simulations of Figure 4 were 26 nm for 3a, 100nm for 3b, 74nm for 3c, and 28nm for 3d. These CBED results permit identifying the polarity of the surfaces in relation to the shapes and orientations of the etched voids.

Figures 3a and 3c−e show that the [000$\bar{1}$] direction always pointed to the larger flat side of each void perpendicular to the *c*-axis. All etched ZnO nanostructures investigated in the present work yielded the same results. This indicates that ZnO nanostructures exhibit consistent etching behavior in SPS. Figures 5a,b are HRTEM images of the voids viewed

Table 2. Comparison of Methods for Identifying the Polarity of ZnO Nano Crystals

methods	CBED [32]	HRTEM [34]	EELS [35]	CE
process	record CBED patterns; compare with the simulated patterns.	record HRTEM images; compare with atomic model.	collect EELS spectra; compare element peak intensities.	directly observe by TEM
real-time	no	no	no	yes
sample geometry	thickness >10 nm. flat and free of defects.	thickness <5 nm. flat and free of defects.	proper thickness.	no limit.
equipments	normal TEM	HRTEM	special EELS	normal TEM
time consuming	yes	yes	yes	no
reliability	high	low	high	high
feasibility for bulk quantity of samples	no	no	no	yes

along the [1$\bar{1}$00] and [11$\bar{2}$0] directions, respectively. The 3D structure of the voids can be deduced by analyzing the image contrast. Figures 5c,d illustrate the thickness changes of the void along the observing direction. Because a thin foil gives an intense image, the reversion of the profile in areas A and B reveals different concave shapes in the voids. Figure 6 shows the structure of the etched voids. The voids are enclosed by the {01$\bar{1}$1} and ±(0001) planes, with the sequence of areas $S_{(000\bar{1})} > S_{\{10\bar{1}1\}} > S_{(0001)}$. This indicates anisotropic etching at speeds along different directions $V_{\langle 0001\rangle} > V_{\vec{n}\perp\{10\bar{1}1\}} > V_{[000\bar{1}]}$ ($\vec{n}$ stands for the normal direction of the planes). This relationship of etching speeds is consistent with ZnO's growth speeds along different directions in neutral solution ($V_{<0001>} > V_{\vec{n}\perp\{10\bar{1}\bar{1}\}} > V_{\vec{n}\perp\{10\bar{1}1\}} > V_{[000\bar{1}]}$) as observed by Li et al. [33] Because the etching behavior of ZnO crystals in SPS is due to the anisotropy of ZnO crystals and independent of the morphology of the ZnO nanostructure, the observed behavior can be used to determine the polar directions, especially the [0001] and [000$\bar{1}$] directions. This is important for understanding the growth of nanosized crystals dominated by polar surfaces. By immersing a sample in SPS and examining it with TEM, the polar directions can be identified immediately from the shapes of the etched voids. The immersion time can be shortened to several hours at an elevated etching temperature.

Currently, three TEM techniques are widely applied for determining the polar surfaces of ZnO nanostructures: (1) CBED,[25–27,32] (2) HRTEM, [34] and (3) the electron energy loss spectrum (EELS) technique.[35] Table 2 compares these three methods. The key requirement for forming a high quality CBED pattern is a sample thicker than one extinction distance (about 100 nm at 120 kV) to give a strong dynamic effect. Samples in nanostructure studies are always thinner than 100 nm. In this situation, low accelerating voltages for the electron beam and a cooling holder are used to improve contrast and increase the number of the Kossel−Moellenstedt fringes (or decrease the extinction distance in the material). The identification process is time-consuming and is not useful for the samples less than 10 nm thick. In addition, this method is very sensitive to the defects in the sample. Identifying the polar direction using HRTEM largely depends on the quality of the HRTEM images and the image simulation, as has been discussed by Ding et al.[34] Moreover, the orientation of the nanocrystals severely limits the applicability of this technique. Compared to CBED, the advantage of HRTEM is that it can be used to study samples less than 10 nm thick. The EELS method determines the polar directions by comparing the element peak intensities in the EELS spectra collected at two beam conditions with proper collection angles. The experimental procedure is complicated, requiring a dedicated and skilled operator, and the results are very sensitive to factors such as contamination, the thickness of the sample, and collection angles.[35]

The chemical etching (CE) method proposed in the present work is, by contrast, relatively simple, reliable, timesaving, and easy to manipulate, with less constraints on sample geometry and preparation, equipment, and technique. It can be used to investigate many samples quickly for any sample thicknesses and growth direction. In addition, this method might be applied to other polar crystals if a proper etching solution is chosen. The chemical stability of ZnO nanostructures in SPS has important implications for medical applications. ZnO can potentially be used in biosensors, where a reasonable exposure time is often required for sensing in biological systems. Indeed, working times from several hours to several days or even several weeks are often needed. In addition, the behavior of ZnO nanostructures in vivo is often similar to that of many bioactive materials, which could potentially allow its use in many applications.[36,37]

Acknowledgment. The authors are grateful for the technical assistance of Mr. T. K. Zhang and Mr. K. M. Ho of the Department of Physics, HKUST. This work was financially supported by the Research Grants Council of Hong Kong (Project Nos. N_HKUST615/06, 603006 and CA04/05.SC04).

IC8005234

(32) Wang, Z. L.; Kong, X. Y.; Zuo, J. M. *Phys. Rev. Lett.* **2003**, *91*, 185502.
(33) Li, W. J.; Shi, E. W.; Zhong, W. Z.; Yin, Z. W. *J. Cryst. Growth* **1999**, *203*, 186.
(34) Ding, Y.; Wang, Z. L. *Surf. Sci.* **2007**, *601*, 425.
(35) Zhang, Z. H.; Liu, H. H.; Jian, J. K.; Zou, K.; Duan, X. F. *Appl. Phys. Lett.* **2006**, *88*, 193101.
(36) Kenny, S.; Hill, R. G.; Towler, M. J. *Mater. Sci: Mater. Med.* **2000**, *11*, 847.
(37) Kenny, S.; Buggy, M.; Hill, R. G. J. *Mater. Sci: Mater. Med.* **2001**, *12*, 901.